Characterization of nanostructured CuO thin films grown with microwave activated chemical bath deposition when process is repeated for thickness increase

C.Laza[1], I.Zumeta[2], D. Ferrera[3], B. González[1], O.Estevez[1], F. Forcade[1], E. Vigil[4]*

[1] Instituto de Ciencia y Tecnología de Materiales, Universidad de la Habana, La Habana (Cuba)

[2]Centro de Investigación y de Estudios Avanzados del Instituto Politécnico Nacional, D.F (México)

[3]Facultad de Química, Universidad de la Habana, Habana (Cuba)

[4]Facultad de Física, Universidad de la Habana, Habana (Cuba)

Abstract

Nanostructured CuO shows perspectives as solar cell and water splitting material because of bandgap value and properties dependence on the employed technology. CuO films deposited with microwave activated chemical bath deposition show interesting nano-morphology and characteristics. This technique is simple and inexpensive; it requires less than 5-minute-long deposition time plus temperature below 75 ºC - conditions desirable for solar energy capture devices. When processes are repeated for thickness increase, important changes of CuO films characteristics occur. X-ray diffraction and Raman spectroscopy reveal morphological and structural properties. Optical transmission and reflection experiments demonstrate corresponding changes in bandgap value.

Keywords: Nanostructured CuO, MW-CBD, solar cell, water splitting

1. Introduction

CuO nanostructured films are currently studied for applications in solar cells (Wu et al, 2018) and water splitting (Li et al, 2019). Material characteristics depend on nano-morphologies which result from different deposition technologies and bandgap increases from 1.2 eV to over 1.5 eV (Ray et al, 2017) when nanocrystal size decreases. This makes nano-CuO very interesting for band engineering required to improve solar devices characteristics. On the other hand, novel microwave-activated chemical bath deposition (MW-CBD) allows semiconductor growth rather than deposition on the FTO conducting glass due to preferential heating of the substrate, which creates a temperature gradient (Rassaei et al, 2009). MW-CBD allows to grow films at temperatures below 100 ºC and in less than 5 minutes (Gonzalez et al, 2020). MW-CBD is employed to grow CuO films using one, two and three microwave processes to increase layer thickness. Their characteristics are analyzed using optical transmittance, diffused reflection, scanning electron microscopy (SEM), X-ray diffraction (XRD) and Raman spectroscopy

2. Experimental part

2.1 Samples preparation

Copper oxide films were deposited on FTO conducting glass (TEC-15 – Pilkington). FTO pieces (2.0×1.5 cm^2) were cleaned ultrasonically with 2-propanol and then with distilled water (during 3 minutes each). The precursor solution was prepared by mixing 1 part of 0.2 M Cu (II) acetate aqueous solution and 9 parts of ethylene glycol (boiling temperature T = 197.6 °C). The substrate was placed vertically in 15 cm^3 of the precursor solution at the center of a microwave oven working at 2.45×10^9 Hz (cavity volume: 28×28×21 cm^3). The glass with the precursor solution and substrate was placed at the center of another glass filled with water; this one has a larger diameter in order to regulate temperature. The microwave power used was 0.7 kW. To guarantee direct growth on the substrate, microwave irradiation was applied during a short time while no nucleation in the precursor solution appeared. Continuous microwave irradiation time did not exceed 2 minutes. The deposition process could be repeated to obtain thicker layers, always starting from room temperature. The precursor solution temperature after microwave irradiation never exceeded 75 °C as measured with a digital infrared thermometer. Following the MW-

doi:10.18086/swc.2021.06.01 Available at http://proceedings.ises.org

CBD process, the sample was rinsed and sonicated in distilled water. Finally, the sample was heat treated in air at T = 450 ± 50 °C during one hour to guarantee full oxidation to CuO.

To analyze technology effects different sample types were fabricated using 0.2M or 0.1M $Cu(AcO)_2$ solution concentration and pH6 or pH7 of the precursor solution. Samples were identified by ST, 1CT, 2CT and 3CT for one MW-CBD process but no heat treatment, one MW-CBD plus heat treatment, two MW-CBD plus heat treatment and three MW-CBD plus heat treatment, respectively. The sample number follows this ID plus pH and $Cu(AcO)_2$ solution concentration values.

2.2 Samples characterization

The X-ray diffraction (XRD) pattern was obtained in a Bruker diffractometer, D2-Phaser model, on Bragg-Brentano condition using the $K_{\alpha 1}$ radiation of copper and a Lynx-eye detector. The Raman spectrum was recorded in a Thermo Scientific DXR Raman Microscope equipment using laser radiation of 455 nm and 0.5 mW of power, focused by a 50X objective with 0.75 of numerical aperture, integration time of 5 s per scan and 10 scans per spectrum. Optical transmission and reflection spectra were obtained in a Cary 5000 UV-Vis-NIR spectrophotometer, Agilent, equipped with a "Praying Mantis" accessory.

3. Results and discussion

Figure 1 shows photos of typical CuO thin films obtained using MW-CBD. The first lighter color one corresponds to a film obtained using one MW-CBD process and no heat treatment. After heat treatment a one-process sample becomes darker (second photo). This could be due to Cu species that were not fully oxidized to CuO or to quantum size effects. This will be discussed later. Even darker samples are obtained when using more than one MW-CBD process and heat treatment. This is due to sample thickness increase as further experiments also show. Samples shown were obtained with a 0,2M $Cu(AcO)_2$ concentration and pH6 of the precursor solution. Gradual darkening with heat treatment and number of processes is also observed when using other concentration and pH values.

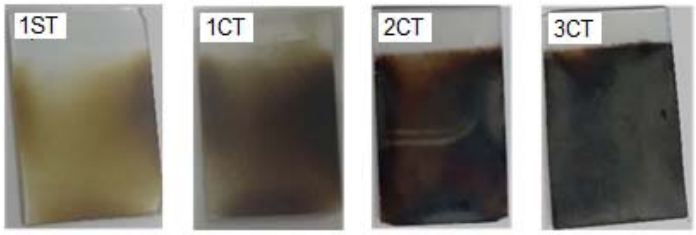

Fig. 1: Films obtained using microwave-activated chemical bath deposition. The 1ST sample has no heat treatment. The first digit indicates the number of MW-CBD processes. Samples shown were obtained with a 0,2M $Cu(AcO)_2$ concentration and pH6 of the precursor solution.

In figure 2 scanning electron microscopies show the grain morphology of CuO films obtained when using MW-CBD. One can observe that the grain size increases when using a more concentrated $Cu(AcO)_2$ solution.

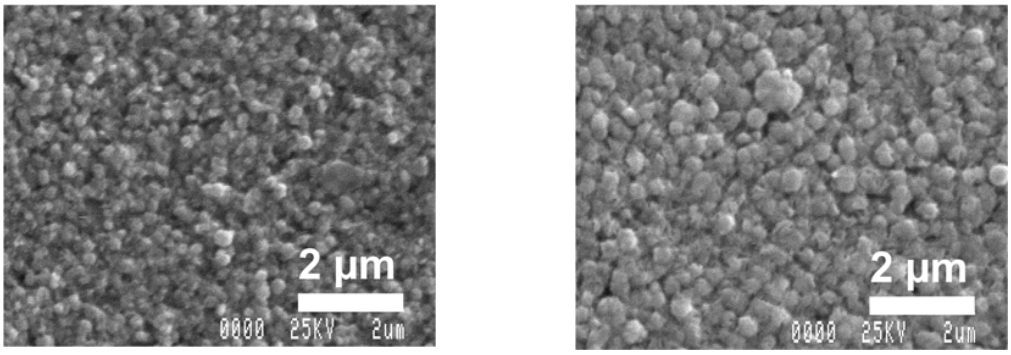

(a) (b)

Fig. 2: Scanning electron microscopy (SEM) images (a) concentration of $Cu(AcO)_2$ solution 0.1 mol/l (1CT-P46-pH6-0.1), (b) concentration of $Cu(AcO)_2$ solution 0.2 mol/l (1CT-P8-pH6-0.2)

In figure 3 one can observe that typical optical transmittance experiments for a single process, with and without heat treatment, plotted as log T^{-1} show practically no light absorption in the 500-800 nm range where CuO absorbs light (log T^{-1} is not exactly equal to optical absorption due to reflection losses, which should be relatively small). This could mean that Cu_2O is deposited first, rather than CuO but this could not be true for one-process samples with heat treatment above 450 ^{0}C. At this temperature, Cu_2O necessarily oxidizes to CuO. Then, quantum size effects due to fine nano-morphology requiring higher SEM resolution (see Gonzalez et al, 2020) could explain it. Films made with two and three MW-CBD processes plus heat treatment show a higher absorption. This indicates that thicker films are obtained. One can observe also, that curves show optical absorption starting at higher wavelengths (lower energies) for samples with three MW-CBD processes. It is well known that the absorption edge depends on the bandgap value.

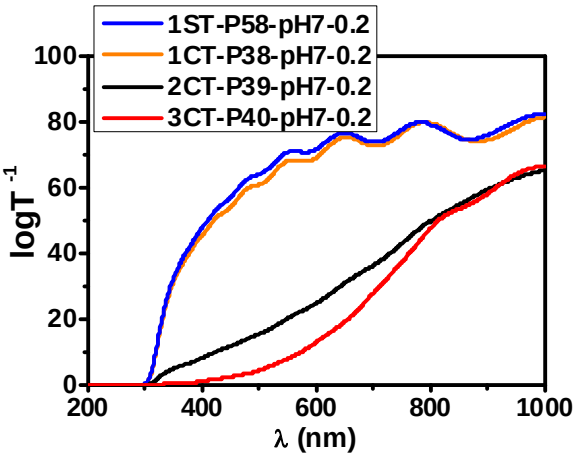

Fig. 3: Typical dependence of log T^{-1} with wavelength from transmittance experiments which allows to analyze light absorption by films. Spectra correspond to samples 1ST-P58-pH7-0.2, one MW-CBD but no heat treatment; 1CT-P38-pH7-0.2, one MW-CBD with heat treatment; 2CT-P39-pH7-0.2, two MW-CBD with heat treatment; 3CT-P40-pH7-0.2, three MW-CBD with heat treatment

The Kuvelka-Munk function F(R) obtained from diffused reflection spectra, is shown in figure 4 for samples with different number of MW-CBD processes and fabricated using precursor solution with concentration 0.2 M $Cu(AcO)_2$ and pH6. The wavelength value at which samples start reflecting significantly increases with the number of processes indicating different bandgap values.

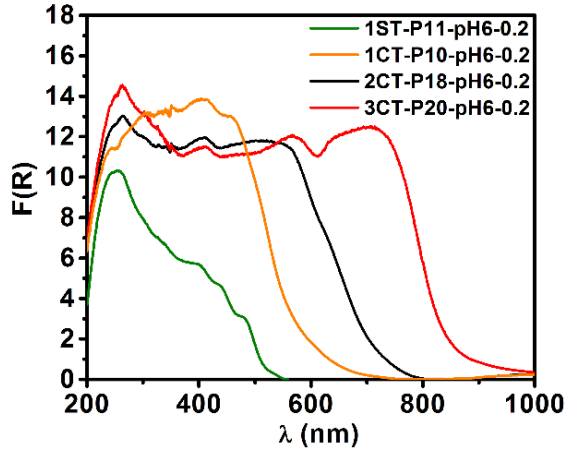

Fig. 4: Kubelka-Munk function F(R) obtained from diffused reflectance experiments for samples with a different number of processes: 1ST-P11-pH6-0.2, one MW-CBD but no heat treatment; 1CT-P10-pH6-0.2, one MW-CBD with heat treatment; 2CT-P18-pH6-0.2, two MW-CBD with heat treatment; 3CT-P20-pH6-0.2, three MW-CBD with heat treatment

From diffused reflectance experiments, using Kubelka-Munk procedure, energy bandgap values were obtained from the plot of $[\mathbf{h\nu} * \boldsymbol{F(R)}]^2 = \boldsymbol{A}(\mathbf{h\nu} - \boldsymbol{E_g})$ (see Table 1). Results indicate a direct bandgap as expected for CuO and values agree with those reported for nanostructured CuO (Zhang, et al, 2014).

Tab. 1: Energy bandgap for films from different number of MW-CBD processes (0.2M $Cu(AcO)_2$ concentration and pH6)

Number of MW-CBD processes	Sample	Bandgap (eV)
One, no heat treatment	1ST-P11-pH6-0.2	2.45
One plus heat treatment	1CT-P10-pH6-0.2	2.28
Two plus heat treatment	2CT-P18-pH6-0.2	1.83
Three plus heat treatment	3CT-P20-pH6-0.2	1.53

As observed in Table 1, values increase for samples with a lower number of MW-CBD processes. This is consistent with the presence of quantum size effects due to very fine nanomorphology and it should be studied further with higher resolution scanning electron microscopy (with a higher number of processes nanocrystal size may increase). Nonetheless, the possibility of controlling CuO gap value using MW-CBD is quite interesting for band engineering.

Typical Raman spectra corresponding to films with a different number of processes are shown in figure 5. As can be seen, the characteristic Raman active modes of monoclinic CuO (tenorite) at 296 cm^{-1} (A_g), 446 cm^{-1} (B_g^1) and 631 cm^{-1} (B_g^2) are present, in accordance with previous reports (Debbichi, et al, 2012). Both Raman active modes only include movement of oxygen anions, with copper cations in almost fixed positions (in A_g mode the anions displace along the (010) direction while in B_g modes the anions displace perpendicular to the (010) direction (Ekuma, et al, 2014).

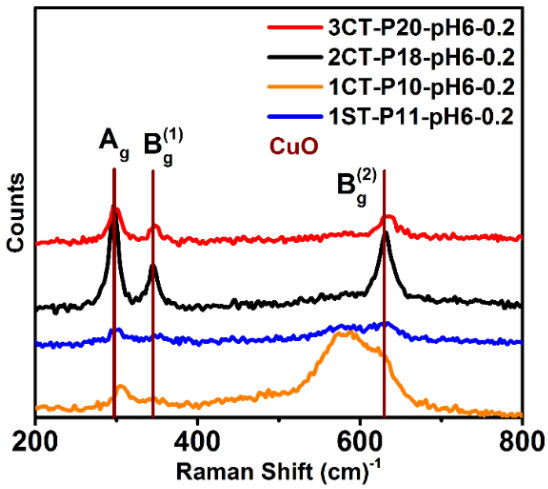

Fig. 5: Raman spectra for samples with different number of MW-CBD processes: 1ST-P11-pH6-0.2, one MW-CBD but no heat treatment; 1CT-P10-pH6-0.2, one MW-CBD with heat treatment; 2CT-P18-pH6-0.2, two MW-CBD with heat treatment; 3CT-P20-pH6-0.2, three MW-CBD with heat treatment

Only pure CuO is detected as film component. Spectra evolution shows that crystallinity increases with the number of processes since the wider the Raman peaks, the higher the crystal disorder. This is also consistent with an increase of nanocrystal size; the higher this size, the lesser disorder. The wide peak below 600 nm^{-1} can be associated to the FTO substrate. It decreases as film thickness increases since laser light intensity does not reach the FTO substrate when thicker CuO films absorb it.

Typical XRD patterns corresponding to films with a different number of processes are shown in figure 6. All XRD patterns show mainly FTO substrate diffraction peaks, which match with the PDF 41-1445 of Cassiterite SnO_2. Only XRD patterns corresponding to films with two and three processes show three relatively broad peaks that fairly match the PDF 48-1548 that corresponds to the tenorite CuO phase (monoclinic system). No other copper-based material was detected by XRD.

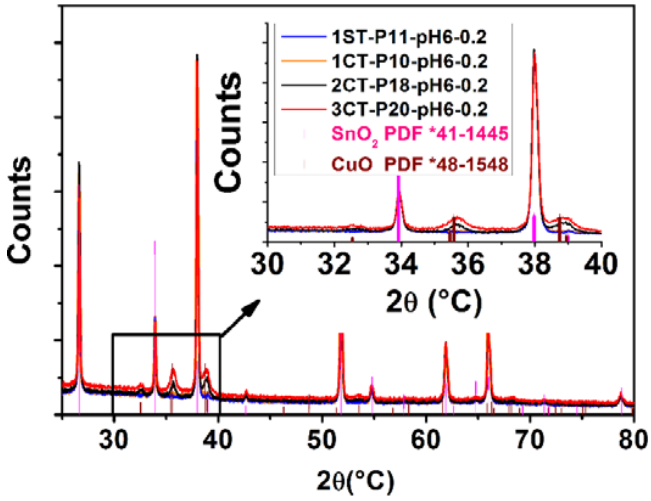

Fig 6: XRD patterns corresponding to samples with different number of processes: 1ST-P11-pH6-0.2, one MW-CBD but no heat treatment; 1CT-P10-pH6-0.2, one MW-CBD with heat treatment; 2CT-P18-pH6-0.2, two MW-CBD with heat treatment; 3CT-P20-pH6-0.2, three MW-CBD with heat treatment. The insert shows peaks corresponding to CuO.

The insert in figure 6 shows peaks corresponding to CuO. These peaks are at: 32.58º, corresponding to the (110) plane; 35.68º, with contributions from the (002) and (11-1) planes; and 38.88º, resulting from the (111) and (200) planes. Relative intensities of these three peaks are quite close to those of the reference (PDF 48-1548), but their relative intensities do not match that of the rest of the peaks in that reference. For instance, peaks at 48.76º, 61.58º, 66.28º and 68.19º are not present in the XRD pattern in figure 6 but their intensities should be higher than that of the (110) plane. This indicates preferential growth that could be induced by the FTO substrate.

It can also be noted that the peaks present in the patterns of 2CT-P18-pH6-0.2 and 3CT-P20-pH6-0.2 samples are slightly shift to higher diffraction angles, with respect to those of the reference, indicating some degree of lattice parameters contraction. Increase in surface/interface stress due to incomplete atomic coordination in such lattice discontinuities has been identified as the main factor for cell parameter contraction in CuO and other nanostructures (Borgohain et al, 2000).

Figure 7 shows Raman spectra of CuO films fabricated with different pH values of the precursor solutions but equal number of MW-CBD processes and the same concentration of the $Cu(AcO)_2$ solution. It is important that only with these two pH values, pH6 and pH7, CuO films MW-CBD was possible. For more acidic precursor solutions, films did not deposit and for higher pH values, a precipitate formed in the solution without MW-CBD.

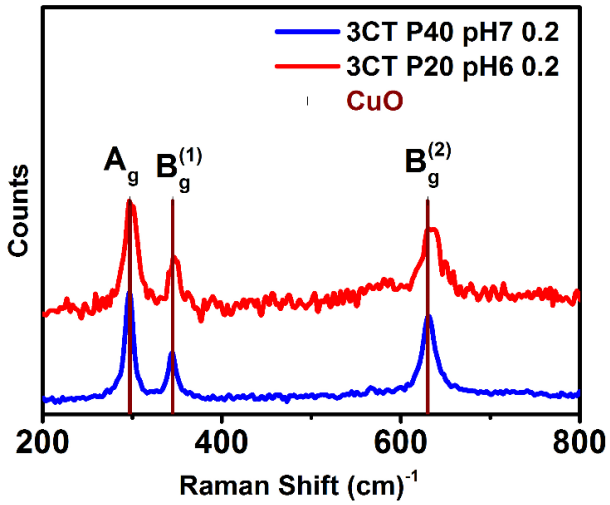

Fig 7: Raman spectra corresponding to films fabricated with precursor solution pH6 and pH7. Both samples, 3CT-P20-pH6-0.2 and 3CT-P40-pH7-0.2, endured three MW-CBD processes with heat treatment. Equal concentration of the $Cu(AcO)_2$ solution was used.

One can observe that Raman spectra for pH7 are better defined than for pH6. This indicates a higher degree of

crystallinity consistent with larger nanocrystal size. In addition, one can notice different intensity relations between peaks A_g and B_g^1. This might be due to preferential growth in a certain nanocrystal direction and it might be observed with higher resolution scanning electron microscopy (Gonzalez, et al, 2020).

Figure 8 shows XRD patterns of CuO films fabricated with different pH values of the precursor solutions but equal number of MW-CBD processes and the same concentration of the $Cu(AcO)_2$ solution. One can observe that CuO peaks are better defined when using precursor solution with pH7.

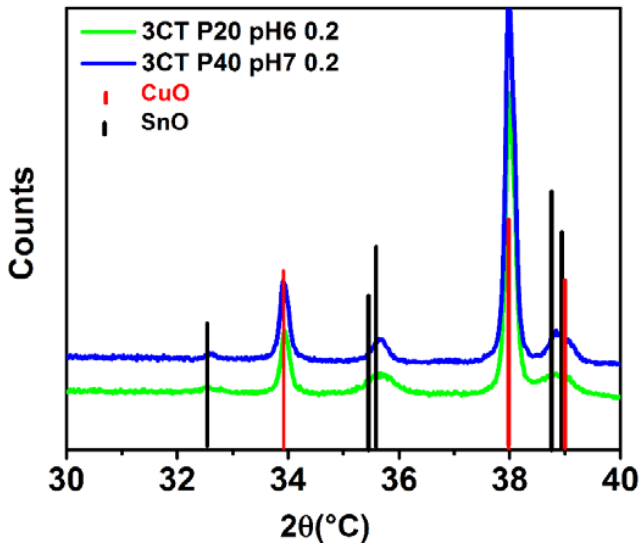

Fig 8: XRD patterns corresponding to films fabricated with precursor solution pH6 and pH7. Both samples, 3CT-P20-pH6-0.2 and 3CT-P40-pH7-0.2, endured three MW-CBD processes with heat treat<<ment. Equal concentration of the $Cu(AcO)_2$ solution was used.

For films in figure 8, it was possible to find crystallite size applying Scherrer analysis to the peak at 32.6º which is produced by diffraction of the (110) plane. This is the only well-resolved peak because only diffraction from one crystal plane contributes. In Table 2 one can observe a smaller value for the full width at half maximum (FWHM) of the sample fabricated with pH7 of the precursor solution; therefore, crystallite size is significantly larger in this case. Larger n<<anocrystal size implies higher crystallinity and explains the better definition obtained for XRD patterns (and Raman spectra, as well) when using pH7.

Tab. 2: Crystallite size D of films fabricated with precursor solution pH6 and pH7

Film	2θ (°)	FWHM (°)	D (nm)
3CT-P20-pH6-0.2	32.6	0.46	18
3CT-P40-pH7-0.2	32.6	0.21	39

Figure 9 shows Raman spectra of CuO films fabricated with different concentrations of the $Cu(AcO)_2$ solution but the same number of MW-CBD processes and equal pH value of the precursor solution. Both Raman spectra in figure 9 show characteristic vibrational modes for monoclinic CuO. Only a broad shoulder below the vibrational mode $B_g^{(2)}$ does not correspond to monoclinic CuO. This shoulder could be a contribution from the FTO substrate. Thicker films would make less noticeable this shoulder for samples fabricated with the higher concentration value.

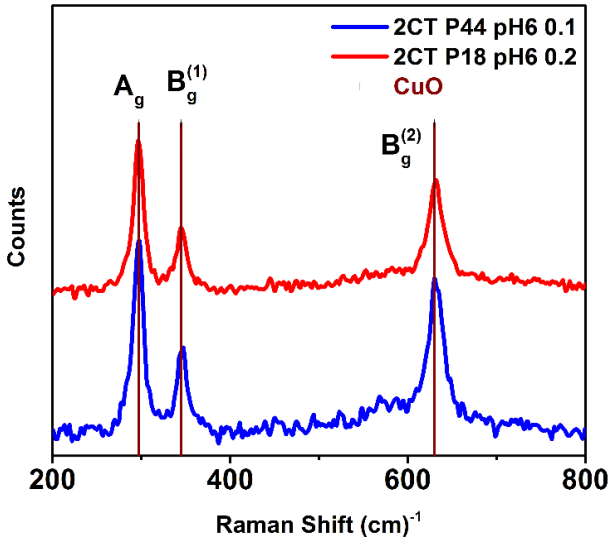

Fig 9: Raman spectra corresponding to films fabricated with different concentrations of the $Cu(AcO)_2$ solutions. 0.1M and 0.2M. Both samples, 2CT-P44-pH6-0.1 and 2CT-P18-pH6-0.2, endured two MW-CBD processes with heat treatment. Equal pH value of the precursor solution was used.

The better defined Raman peaks for the film fabricated using the 0.2M $Cu(AcO)_2$ solution indicate increased crystallinity for this concentration value.

Figure 10 shows XRD patterns for samples fabricated with 0.1M and 0.2M $Cu(AcO)_2$ solution concentrations. Better defined CuO diffraction peaks are observed for films fabricated using 0.2M $Cu(AcO)_2$ concentration. XRD patterns, as well as Raman spectra, show that higher crystallinity films and/or thicker films are obtained for films fabricated using 0.2M $Cu(AcO)_2$ solution concentration.

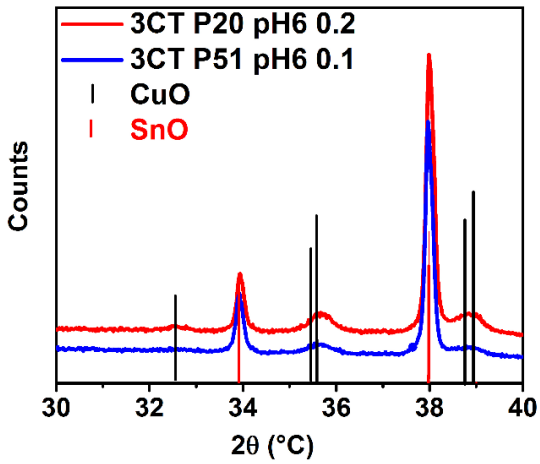

Fig 10: XRD patterns corresponding to films fabricated with different concentrations of the $Cu(AcO)_2$ solutions, 0.1M and 0.2M. Both samples, 3CT-P51-pH6-0.1 and 3CT-P20-pH6-0.2, endured three MW-CBD processes with heat treatment. Equal pH value of the precursor solution was used.

4. Conclusions

CuO films have been deposited on conducting glass (FTO) by means of a novel liquid phase deposition technique named microwave activated chemical bath deposition (MW-CBD). Different procedure conditions have been used for analysis of this technology when growing CuO films. The number of MW-CBD processes performed for each film studied varies from one to three. The employed precursor solutions have different copper (II) acetate solution concentrations and pH values.

All deposited films show very good adherence to the conducting glass (FTO), with deposition times shorter than 5 minutes and precursor solution temperature below 75 ºC. Microwave heating of the conducting substrate during

the process is determinant since it causes an FTO temperature higher than the precursor solution temperature. CuO grows directly on the substrate rather than been deposited from a nucleated precursor solution.

X-ray diffraction and Raman spectroscopy show that only the CuO tenorite phase is present. They all show wide peaks that indicate crystal disorder corresponding to nanostructured morphologies. Film crystallinity improves with the number of processes, higher $Cu(AcO)_2$ concentration and pH7 of the precursor solution.

Behavior of optical transmission and absorption spectra confirms that film thickness grows for each deposition process.

Kubelka-Munk treatment of diffused reflection spectra show that gap energy decreases with the number of processes indicating quantum size effects. This is consistent with observations from XRD patterns and Raman spectra.

Perspective control of crystallinity (nano-crystal size) and bandgap value with this simple, low cost, MW-CBD technique is of importance for band engineering. This is needed for certain devices, particularly solar cells and water splitting photoelectrodes.

References

Borgohain, K., Singh, J. B., Rama Rao, M. V., Shripathi, T., Mahamuni, S., 2000. Quantum size effects in CuO nanoparticles. Phys. Rev. B: Condens. Matter Mater. Phys. 61, 11093 —11096.

Debbichi, L., Marco de Lucas, M. C., Pierson, J. F., Krüger, P., 2012. Vibrational Properties of CuO and Cu4O3 from First-Principles Calculations, and Raman and Infrared Spectroscopy. J. Phys. Chem. C 116, 10232−10237.

Ekuma, C. E., Anisimov, V. I., Moreno, J. and Jarrel, M., 2014. Electronic Structure and Spectra of CuO, Eur. Phys. J. B 87, 23.

Gonzalez, B., Zumeta, I., Díaz-Solís, M., Hernández-Torres, J., Zamora-Peredo, L., Vigil E., 2020. Nanostructured CuO film grown from solution by preferential microwave heating of the conducting glass substrate, Materials Letters 270, 127687.

Li, J., Jin, X., Li, R., Zhao, Y., Wang, X., Liu, X., Jiao H., 2019. Copper oxide nanowires for efficient photoelectrochemical water splitting. Applied Catalysis B: Environmental 240, 1-8.

Rassaei, L., Vigil, E., French, R. W., Mahon, M. F., Compton, R. G., Marken, F., 2009. Effects of microwave radiation on electrodeposition processes at tin-doped indium oxide (ITO) electrodes. Electrochimica Acta 54, 6680–6685.

Ray, A., Mukhopadhyay, I., Pati, R., Hattori, Y., Prakash, U., Ishii, Y., Kawasaki, S., 2017. Optimization of photoelectrochemical performance in chemical bath deposited nanostructured CuO, Journal of Alloys and Compounds 695, 3655-3665.

Wu, F., Qiao, Q., Bahrami, B., Chen, K., Pathak, R., Tong, Y., Li, X., Zhang, T., Jian, R., 2018. Solution-processed all-oxide bulk heterojunction solar cells based on CuO nanorod array and TiO2 nanocrystals. Nanotechnology 29, 215403.

Zhang, Q, Zhang, K., Xu, D., Yang, G., Huang, H., Nie, F., Liu, C., Yang, S., 2014. CuO nanostructures: Synthesis, characterization, growth mechanisms, fundamental properties, and applications. Progress in Materials Science 60, 208-337